

tuted 60 to 65% of the total material in the library (Fig. 4B). Similarly, host **7** can be produced in >95% yield from a small library prepared by oxidizing dithiol **1** in the presence of guest **5** (Fig. 4D). In the absence of the guest, this trimeric host is produced in only 6% yield (Fig. 4C).

These yields are impressive for macrocyclization reactions, which are notorious for producing only small quantities of the desired ring size. Note also that the high-dilution conditions normally required for macrocyclizations are not necessary in these thermodynamically controlled templated syntheses.

We have isolated hosts **6** (major diastereomer) and **7** (mixture of stereoisomers) using preparative HPLC (SOM) and studied the interaction with guests **4** and **5** using ESI-MS and microcalorimetry. The 1:1 host-guest complexes could be detected as main peaks in the mass spectrum together with the free hosts (fig. S1). Binding constants, enthalpies, and entropies obtained by microcalorimetry (fig. S2) are shown in Table 1. The binding constants for the optimal host-guest pairs (**4**·**6** and **5**·**7**) are 6 to 25 times higher than those for the mismatched pairs (**4**·**7** and **5**·**6**). Apparently, the guests can select a tightly binding host from a number of closely related structures. Most importantly, relatively small differences in binding energies are sufficient to lead to large differences in extent of amplification.

Thermodynamic analysis shows that binding is invariably enthalpy-driven and counteracted by entropy, suggesting that binding is dominated by electrostatic interactions including cation- π interactions (26, 27) and possibly also salt-bridge formation. To substantiate this hypothesis, we are currently studying the binding thermodynamics of a wider range of guests. The results of these studies will be reported in due course.

Our results establish dynamic combinatorial chemistry as a powerful and practical tool for the discovery of artificial receptors. Subtle differences in affinity lead to useful differences in amplification. Moreover, the underlying dynamic chemistry can be used directly for large-scale preparations. Reversibility ensures that side products are recyclable, allowing, at least in theory, complete conversion into the desired product even in systems where the templating efficiencies are much smaller than those described herein.

References and Notes

1. S. Otto, R. L. E. Furlan, J. K. M. Sanders, *Drug Discov. Today* **7**, 117 (2002).
2. J. M. Lehn, A. V. Eliseev, *Science* **291**, 2331 (2002).
3. B. Klekota, B. L. Miller, *Trends Biotechnol.* **17**, 205 (1999).
4. S. J. Rowan, S. J. Cantrill, G. R. L. Cousins, J. K. M. Sanders, J. F. Stoddart, *Angew. Chem. Int. Ed.* **41**, 898 (2002).
5. P. A. Brady, R. P. Bonar-Law, S. J. Rowan, C. J. Suckling, J. K. M. Sanders, *Chem. Commun.* 319 (1996).

6. H. Hioki, W. C. Still, *J. Org. Chem.* **63**, 904 (1998).
7. I. Huc, J. M. Lehn, *Proc. Natl. Acad. Sci. U.S.A.* **94**, 2106 (1997).
8. S. Sakai, Y. Shigemasa, T. Sasaki, *Bull. Chem. Soc. Jpn.* **72**, 1313 (1999).
9. M. Crego Calama, P. Timmerman, D. N. Reinhoudt, *Angew. Chem. Int. Ed.* **39**, 755 (2000).
10. R. L. E. Furlan, Y. F. Ng, G. R. L. Cousins, J. E. Redman, J. K. M. Sanders, *Tetrahedron* **58**, 771 (2002).
11. G. R. L. Cousins, R. L. E. Furlan, Y. F. Ng, J. E. Redman, J. K. M. Sanders, *Angew. Chem. Int. Ed.* **40**, 423 (2001).
12. R. L. E. Furlan, Y. F. Ng, S. Otto, J. K. M. Sanders, *J. Am. Chem. Soc.* **123**, 8876 (2001).
13. R. L. E. Furlan, G. R. L. Cousins, J. K. M. Sanders, *Chem. Commun.* 1761 (2000).
14. V. Berl, I. Huc, J. M. Lehn, A. DeCian, J. Fischer, *Eur. J. Org. Chem.* 3089 (1999).
15. I. Huc, M. J. Krische, D. P. Funeriu, J. M. Lehn, *Eur. J. Inorg. Chem.* 1415 (1999).
16. E. Stulz, Y.-F. Ng, S. M. Scott, J. K. M. Sanders, *Chem. Commun.* 524 (2002).
17. J. S. Moore, N. W. Zimmerman, *Org. Lett.* **2**, 915 (2000).
18. S. Otto, R. L. E. Furlan, J. K. M. Sanders, *J. Am. Chem. Soc.* **122**, 12063 (2000).
19. O. Ramström, J. M. Lehn, *ChemBiochem* **1**, 41 (2000).
20. S. M. Ngola, P. C. Kearney, S. Mecozzi, K. Russell, D. A. Dougherty, *J. Am. Chem. Soc.* **121**, 1192 (1999).
21. P. C. Kearney et al., *J. Am. Chem. Soc.* **115**, 9907 (1993).
22. D. A. Stauffer, R. E. Barrans, D. A. Dougherty, *J. Org. Chem.* **55**, 2762 (1990).
23. M. A. Petti, T. J. Sheppard, R. E. Barrans, D. A. Dougherty, *J. Am. Chem. Soc.* **110**, 6825 (1988).
24. In a typical experiment, the dithiols (10 mM overall) were suspended in water and 1 equivalent (with respect to the number of carboxylic acids) of a 1.0 M NaOH solution was added. After all dithiol had dissolved, the pH was adjusted to 8.5 and, where appropriate, the guest (5 to 10 mM) was added. The mixtures were then allowed to oxidize and equilibrate for 3 to 5 days by stirring in an open vial. Evaporated water was replenished every day.
25. Dithiothreitol (DTT; 15 mol%), a reagent for the selective reduction of disulfides to thiols, was added to speed up the exchange process.
26. J. C. Ma, D. A. Dougherty, *Chem. Rev.* **97**, 1303 (1997).
27. D. A. Dougherty, *Science* **271**, 163 (1996).
28. P. Boldt, *Chem. Ber.* **100**, 1270 (1967).
29. L. Field, P. R. Engelhardt, *J. Org. Chem.* **35**, 3647 (1970).
30. H. A. Staab, R. G. H. Kirrstetter, *Liebigs Ann. Chem.* 886 (1979).
31. We thank A. R. Fersht and C. M. Johnson for the use of their isothermal titration microcalorimeter and technical assistance. We acknowledge support from the European Union (Marie Curie Fellowship HPMF-CT-1999-00069) and the Royal Society (University Research Fellowship) to S.O., from the Fundación Antorchas and the Consejo Nacional de Investigaciones Científicas y Técnicas (Argentina) to R.L.E.F. and from EPSRC to J.K.M.S.

Supporting Online Material

www.sciencemag.org/cgi/content/full/297/5581/590/DC1

Materials and Methods

Figs. S1 and S2

29 March 2002; accepted 3 June 2002

Band Gap Fluorescence from Individual Single-Walled Carbon Nanotubes

Michael J. O'Connell,¹ Sergei M. Bachilo,¹ Chad B. Huffman,¹ Valerie C. Moore,¹ Michael S. Strano,¹ Erik H. Haroz,² Kristy L. Rialon,¹ Peter J. Boul,¹ William H. Noon,³ Carter Kittrell,¹ Jianpeng Ma,^{3,4} Robert H. Hauge,¹ R. Bruce Weisman,¹ Richard E. Smalley^{1,2*}

Fluorescence has been observed directly across the band gap of semiconducting carbon nanotubes. We obtained individual nanotubes, each encased in a cylindrical micelle, by ultrasonically agitating an aqueous dispersion of raw single-walled carbon nanotubes in sodium dodecyl sulfate and then centrifuging to remove tube bundles, ropes, and residual catalyst. Aggregation of nanotubes into bundles otherwise quenches the fluorescence through interactions with metallic tubes and substantially broadens the absorption spectra. At pH less than 5, the absorption and emission spectra of individual nanotubes show evidence of band gap-selective protonation of the side walls of the tube. This protonation is readily reversed by treatment with base or ultraviolet light.

Single-walled carbon nanotubes are elongated members of the fullerene family (1) that are currently the focus of intense multidisciplinary study because of their unique physical and chemical properties and their prospects for practical applications (2). A major obstacle to such efforts has been the diversity of tube diameters, chiral angles, and aggregation states in nanotube samples obtained from the various preparation methods. Aggregation is particularly problematic because the highly

polarizable, smooth-sided fullerene tubes readily form parallel bundles or ropes with a van der Waals binding energy of ~500 eV per micrometer of tube-tube contact (3, 4). This bundling perturbs the electronic structure of the tubes, and it confounds all attempts to separate the tubes by size or type or to use them as individual macromolecular species. Although efforts from this laboratory (5, 6) and others (7–12) have reported some progress in producing suspensions enriched

in individual fullerene tubes, available samples have still been dominated by small nanotube bundles. What is needed is a procedure that detaches tubes from bundles by physical means, applies a nonperturbing coating to prevent reaggregation, and then removes from the solution any remaining bundles. We describe a method based on vigorous treatment with a sonicator followed by centrifugation, primarily yielding individual fullerene nanotubes in aqueous micellar suspensions.

Freed from the perturbation of surrounding tubes and surfaces, the tubes in these suspensions show much better resolved optical absorption spectra. Most importantly, the one-dimensional direct band gap semicon-

ducting tubes in these samples are now found to fluoresce brightly in the 800- to 1600-nm wavelength range of the near infrared, a region important in fiber optic communications and bioimaging.

Raw nanotube product from a high-pressure CO reactor [the HiPco process (13)] was dispersed in 200 ml of aqueous sodium dodecyl sulfate (SDS) surfactant [1% by weight (1 wt %)] by 1 hour of high-shear mixing (Polyscience X-520). The resulting dispersion was then treated in a cup-horn sonicator (Cole Palmer CPX-600) for 10 min at a power level of 540 W. Immediately after sonication, samples were centrifuged (Sovall 100S Discovery Ultracentrifuge with Surespin 630 swing bucket rotor) at 122,000g for 4 hours. The upper 75 to 80% of supernatant was then carefully decanted, leaving micelle-suspended nanotube solutions at a typical mass concentration of 20 to 25 mg/l. For some experiments, these nanotube samples were further processed for competitive wrapping with a polymer (6), simply by adding ~1 wt % of 40-kD poly(vinylpyrrolidone) (PVP) to the SDS suspension. Analysis of samples by atomic force microscopy showed most nanotubes to be 80 to 200 nm long, with an

average length of 130 nm. This length distribution is typical of heavily sonicated fullerene nanotubes from a wide range of sources and is believed to arise from sonication-induced tube cutting. However, spectra of these samples, including Raman features such as strong radial breathing modes (RBM) and the near absence of the "disorder peak" near 1330 cm^{-1} (14), strongly suggest that this sonication has not substantially damaged the tube side walls. Transmission electron microscopy (TEM), x-ray diffraction, and RBM Raman measurements indicate tube diameters between 0.7 and 1.1 nm, which is typical of the single-walled nanotubes made by the HiPco technique (13, 15).

As illustrated by Fig. 1, an individual fullerene nanotube encased in a close-packed columnar SDS micelle has a specific gravity of approximately 1.0, whereas that of an SDS-coated seven-tube bundle is approximately 1.2. Therefore, centrifugation brings bundles to the bottom of the centrifuge tube, leaving a supernatant highly enriched in single nanotubes, even in D_2O (density 1.10 g cm^{-3}). Typical samples also contain 3- to 5-nm diameter iron particles, each coated with 1 or 2 atomic layers of carbon. In SDS micelles, these residual catalyst particles have a density near 2 to 3 g cm^{-3} and thus also sediment out upon centrifugation.

Our SDS suspensions of individual nanotubes were found to be much more stable than suspensions of nanotube bundles produced by milder sonication (5). Samples containing 20 mg/l of nanotubes in 1% SDS survive heating to 70°C, addition of up to 40% methanol, NaCl concentrations up to 200 mM, and MgCl_2 concentrations up to 10 mM for periods of greater than 24 hours without flocculation.

The environment of nanotubes in SDS micelles was modeled through molecular dynamics simulations. We performed computations with the CHARMM package (16) and constant-pressure-constant-temperature algorithm (17), using ambient condition parameters (300 K, 1 atm). A modified TIP3P model (18) was used for the potential function of the water molecules. The nanotube wall was simulated by a smooth cylinder with a van der Waals potential appropriate for the side of aromatic carbon rings. The total simulation run was 0.4 ns. Figure 1C shows a typical snapshot of the cross section of the simulation cell, and Fig. 1D shows the density profiles of key components. The hydrophobic tails of the SDS molecules can adopt a wide range of orientations with respect to the tube. Significant probability is observed for the SDS molecules to bend and even to turn around, i.e., for the carbon atoms to reach the average radial position of sulfur atoms. In addition, the water molecules have a small probability to penetrate into the hydrophobic

¹Department of Chemistry, Rice Quantum Institute, and Center for Nanoscale Science and Technology, ²Department of Physics, ³Department of Bioengineering, Rice University, 6100 Main Street, Houston, TX 77005, USA. ⁴Graduate Program of Structural and Computational Biology and Molecular Biophysics, Verna and Marrs McLean Department of Biochemistry and Molecular Biology, Baylor College of Medicine, One Baylor Plaza, BCM-125, Houston, TX 77030, USA.

*To whom correspondence should be addressed. E-mail: smalley@rice.edu

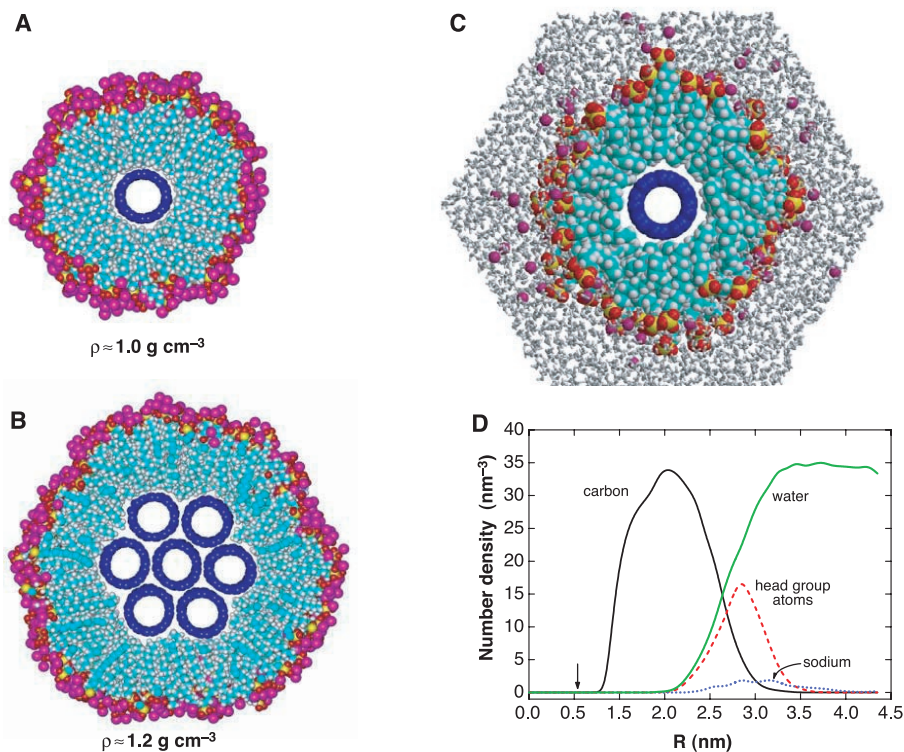


Fig. 1. Cross-section model of (A) an individual fullerene nanotube in a cylindrical SDS micelle and (B) a seven-tube bundle of fullerene nanotubes coated by a layer of SDS. The approximate density of these species is 1.0 and 1.2 g cm^{-3} , respectively. A molecular dynamics simulation of water and the SDS micelle around an individual (8,8) nanotube (C) shows the nanotube as it would exist in a water-free hydrocarbon environment. This figure was prepared using the software Molscrip (32) and rendered by Raster3D (33). (D) The number density profiles for SDS carbon atoms, sulfate head group atoms, water molecules, and sodium ions. The abscissa, R , is measured from the center of the nanotube. The arrow indicates the position of the nanotube wall.

tails, reaching as far as the center of the hydrocarbon distribution. This water penetration is significantly deeper than is found in a simulation of pure cylindrical SDS micelles (19). However, no water density was observed in the direct vicinity of the tube, so individual fullerene nanotubes are essentially in a pure hydrocarbon environment that provides a superb medium for spectral studies.

As is seen in traces A, B, and C of Fig. 2, the electronic absorption spectrum of decanted supernatant samples shows more pronounced structure than the sample of trace D, which was prepared without centrifugation and is apparently dominated by tube bundles. We interpret the spectral structure as a superposition of distinct electronic transitions from a variety of fullerene nanotubes isolated within columnar SDS micelles. Theory predicts that the electronic structure of a single-walled carbon nanotube, including semiconducting versus metallic character, depends on the diameter and chiral wrapping angle describing its construction from a graphene sheet (14). Quasi one-dimensionality causes the electronic density of states to have a series of sharp van Hove maxima at energies dependent mainly on tube diameter. The optical absorption spectrum of a particular tube is expected to be dominated by a series of relatively sharp interband transitions, at energies denoted E_{11} , E_{22} , etc., associated with those van Hove singularities (20). The spectra shown in Fig. 2 are consistent with this expectation, with the first van Hove transitions, E_{11} , of the direct band gap semiconducting tubes falling in the 800- to 1600-nm wavelength range, slightly overlapping the 550- to 900-nm region of their E_{22} transitions. The lowest energy van Hove transitions of the metallic tubes appear between ~ 400 and 600 nm.

Our observed spectra depend systematically on the high-pressure reactor conditions used to make the sample, on the suspending agent, and on the pH of the solution. In traces A and B of Fig. 2, we plotted absorption spectra of two reactor batches made at CO pressures of 50 and 30 atm, respectively, that are known to differ in average tube diameter. The absorption peaks in these two spectra match exactly in wavelength but differ substantially in relative intensity. This indicates that the peaks arise from specific tube species common to both samples, with smaller diameter tubes more abundant in the higher pressure sample, A. Trace C shows that addition of PVP to the SDS micelles causes the peaks at wavelengths beyond 900 nm to red-shift and broaden, reflecting a more polarizable and inhomogeneous environment. Trace D, the spectrum of aggregated nanotubes in SDS micelles, shows features still more red-shifted and so broadened that little structure can be discerned. We attribute this broadening to interactions between bundled tubes in side-by-side van der Waals contact (21).

Acidic solutions with $\text{pH} < 3$ display

absorption spectra containing only broad, unstructured absorption in the first van Hove region, E_{11} . However, the structured spectrum recovers upon neutralizing the solution to $\text{pH} > 7$, and this effect was found to be reproducible for many cycles. We believe that this pH sensitivity reflects reversible side wall protonation of the fullerene nanotubes. The larger diameter (smallest band gap) semiconducting tubes protonate first as pH is decreased and deprotonate last as pH is increased.

In contrast to previous studies (22–26), the individual fullerene nanotube samples were found to display a bright, structured photoluminescence in the near infrared. Figure 3 plots the spectrum of this emission from nanotubes in SDS micelles in D_2O after pulsed laser excitation at 532 nm. Comparison with the overlaid absorption spectrum of the same sample reveals a striking correspondence. Each absorption component in the spectral region of first van Hove “band gap” transition of the semiconducting tubes, E_{11} , is present in the emission spectrum, red-shifted by only $\sim 45 \text{ cm}^{-1}$ (27). Therefore, we assign the emission to semiconducting nanotubes. The individual components of the emission spectrum appear to have widths of approximately 0.025 eV, or 200 cm^{-1} , very close to the value of thermal energy, $k_{\text{B}}T$ for these room temperature samples.

The shortest wavelength emission feature

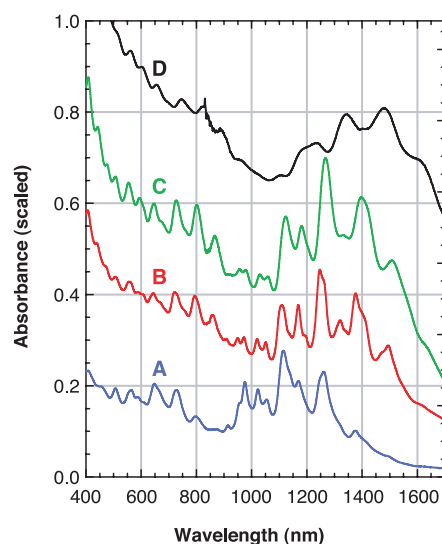


Fig. 2. Absorption spectra of fullerene nanotubes in SDS- D_2O suspension. The top trace D is typical of tubes prepared in suspension without centrifugation. The broadened and red-shifted absorption features show that most nanotubes in the sample are aggregated in small bundles. Trace C is from individual SDS micelle coated nanotubes after addition of PVP. Traces B and A are from samples of individual nanotubes separated and solubilized by SDS micelles. Nanotubes in sample A have a smaller average diameter than in B because they were grown under a higher CO pressure.

in Fig. 3, corresponding to the band gap of the smallest diameter semiconducting nanotube species readily detectable in our sample, peaks near 875 nm (1.42 eV). Given that TEM and Raman studies show the smallest diameter tubes in these HiPco samples to be no smaller than 0.7 nm, our optical E_{11} value is surprisingly large compared with previous scanning tunneling spectroscopy (STS) measurements of the band gaps of selected individual semiconducting tubes on gold surfaces (2, 28, 29).

We find that photoluminescence intensity is dramatically reduced by aggregation of the isolated nanotubes or by acidification of the SDS micellar suspension. Bright emission requires vigorous cup-horn sonication to unbundle aggregates into isolated nanotubes. We presume that the presence of a metallic nanotube within a bundle will quench electronic excitation on an adjacent semiconducting tube, preventing its luminescence. Although the differential sedimentation technique used here may not completely remove micelle-coated small bundles of two or three nanotubes in side-by-side van der Waals contact, the detailed overlap between the fluorescence and absorption spectra shown in Fig. 3 leads us to believe that our samples contain mainly micelle-coated individual tubes. Otherwise, energy transfer within bundles would have shifted much of the emission intensity to longer wavelengths characteristic of the smaller band gap tubes. Emission from SDS-suspended samples is most intense in basic solution, becomes undetectable at pH 3, and is restored above pH 7. Emission peaks at longer wavelengths (from nanotubes with the smallest band gaps) show the strongest sensitivity to acidification. We also find that ultraviolet (UV) light from a low-pressure mercury pen lamp is highly effective in restoring photoluminescence

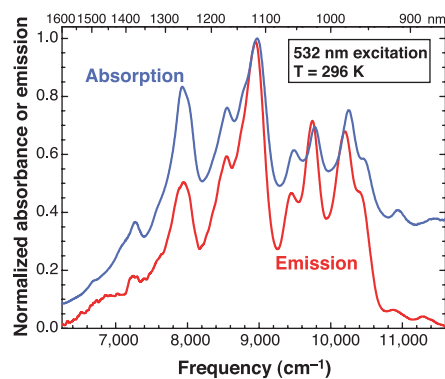


Fig. 3. Emission spectrum (red) of individual fullerene nanotubes suspended in SDS micelles in D_2O excited by 8 ns, 532-nm laser pulses, overlaid with the absorption spectrum (blue) of the sample in this region of first van Hove band gap transitions. The detailed correspondence of absorption and emission features indicates that the emission is band gap photoluminescence from a variety of semiconducting nanotube structures.

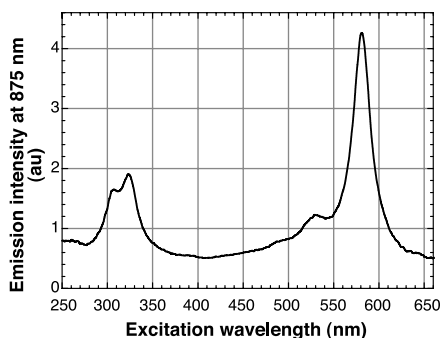


Fig. 4. Fluorescence excitation spectrum of the 875-nm band gap emission feature in a 296 K sample of fullerene nanotubes in 1% SDS in H₂O. The strong excitation feature at 581 nm is assigned as the second van Hove absorption of this nanotube species, appearing at an energy 1.51 times that of the first van Hove transition.

from protonated tubes in SDS micelles. This effect appears similar to the previously reported UV photodesorption of O₂ and other small molecules from single-walled nanotubes (30). PVP-wrapped nanotubes, dissolved either in water or in a solid film of PVP, show band gap luminescence efficiencies comparable to those of SDS-suspended samples.

The characteristic luminescence lifetime is found to be less than 2 ns, and we estimate a quantum yield on the order of 10⁻³. Therefore, we classify the luminescence as fluorescence: spin-allowed emission from singlet excitons. This assignment is consistent with the very small spectral shift between absorption and emission, which also implies only minor geometrical differences between the ground and excited electronic states.

Optical excitation of a semiconducting nanotube in its second van Hove transition, E₂₂, will be followed by rapid electronic relaxation before emission in the first-branch transition, E₁₁. Therefore, by monitoring the intensity of a specific (first-branch) emission peak as a function of excitation wavelength within the second van Hove branch, one can identify the second-branch transition energy of the nanotube that gives that first-branch emission. Figure 4, which illustrates such an excitation spectrum for the 875-nm first-branch emission peak, shows a distinct, nearly lorentzian second-branch feature centered at 581 nm, giving a E₂₂/E₁₁ value for this particular tube of 1.51. Extensive fluorescence excitation measurements, similar to Fig. 4, are now in progress for the entire range of emission features from these micelle-suspended tube samples. Early results show that the E₂₂/E₁₁ ratio varies widely but averages to a value near 1.7, in contrast to the value of 2.0 predicted by tight binding theory (2). This difference may reflect nanotube exciton effects (31).

The observed nanotube fluorescence intensity was found to depend nonlinearly on the excitation intensity. Using 8-ns laser

pulses at 532 nm, we observe that emission increases nearly linearly for energy densities below 0.1 mJ cm⁻² but sublinearly at higher excitation levels, with an emission efficiency at 6 mJ cm⁻² only ~25% of that found for weak excitation. Further studies will be needed to explore this nonlinear behavior, which probably reflects annihilating interactions between multiple excitons on individual nanotubes.

References and Notes

1. M. S. Dresselhaus, G. Dresselhaus, P. C. Klund, *Science of Fullerenes and Carbon Nanotubes* (Academic Press, San Diego, 1996).
2. M. S. Dresselhaus, G. Dresselhaus, P. Avouris, Eds., *Carbon Nanotubes: Synthesis, Structure, Properties, and Applications*, vol. 80 (Springer, Berlin, 2001).
3. A. Thess *et al.*, *Science* **273**, 483 (1996).
4. L. A. Girifalco, M. Hodak, R. S. Lee, *Phys. Rev. B* **62**, 13104 (2000).
5. J. Liu *et al.*, *Science* **280**, 1253 (1998).
6. M. J. O'Connell *et al.*, *Chem. Phys. Lett.* **342**, 265 (2001).
7. S. Bandow *et al.*, *J. Phys. Chem. B* **101**, 8839 (1997).
8. J. Chen *et al.*, *Science* **282**, 95 (1998).
9. G. S. Duesberg, J. Muster, V. Krstic, M. Burghard, S. Roth, *Appl. Phys. A* **67**, 117 (1998).
10. A. B. Dalton *et al.*, *J. Phys. Chem. B* **104**, 10012 (2000).
11. A. B. Dalton *et al.*, *Synth. Metals* **121**, 1217 (2001).
12. R. Bandyopadhyaya, E. Nativ-Roth, O. Regev, R. Yerushalmi-Rozen, *Nano Lett.* **2**, 25 (2002).
13. M. J. Bronikowski, P. A. Willis, D. T. Colbert, K. A. Smith, R. E. Smalley, *J. Vacuum Sci. Technol. A* **19**, 1800 (2001).
14. R. Saito, G. Dresselhaus, M. S. Dresselhaus, *Physical Properties of Carbon Nanotubes* (Imperial College Press, London, 1998).
15. W. Zhou *et al.*, *Chem. Phys. Lett.* **350**, 6 (2001).
16. B. R. Brooks *et al.*, *J. Comput. Chem.* **4**, 187 (1983).

17. S. E. Feller, Y. Zhang, R. W. Pastor, *J. Chem. Phys.* **103**, 4613 (1995).
18. W. L. Jorgensen, *J. Am. Chem. Soc.* **103**, 335 (1981).
19. S. Bandyopadhyay, M. L. Klein, G. Martyna, J. M. Tarek, *Mol. Phys.* **95**, 377 (1998).
20. R. Saito, G. Dresselhaus, M. S. Dresselhaus, *Phys. Rev. B* **61**, 2981 (2000).
21. S. Reich, C. Thomsen, P. Ordejon, *Phys. Rev. B* **65**, 155411 (2002).
22. J. E. Riggs, Z. X. Guo, D. L. Carroll, Y. P. Sun, *J. Am. Chem. Soc.* **122**, 5879 (2000).
23. Y. Sun, S. R. Wilson, D. I. Schuster, *J. Am. Chem. Soc.* **123**, 5348 (2001).
24. E. C. Dickey *et al.*, *Appl. Phys. Lett.* **79**, 4022 (2001).
25. M. E. Brennan *et al.*, *Synth. Metals* **119**, 641 (2001).
26. Y. P. Sun *et al.*, *Chem. Phys. Lett.* **351**, 349 (2002).
27. Such a matched pattern implies a set of chromophores, each lacking vibrational structure in absorption and emission. Vibrational overtone emission would be undetectably weak under our conditions, and organic impurities would not emit in the near infrared.
28. T. W. Odom, J. L. Huang, P. Kim, C. M. Lieber, *Nature* **391**, 62 (1998).
29. J. W. G. Wildoer, L. C. Venema, A. G. Rinzler, R. E. Smalley, C. Dekker, *Nature* **391**, 59 (1998).
30. R. J. Chen *et al.*, *Appl. Phys. Lett.* **79**, 2258 (2001).
31. T. Ando, *J. Phys. Soc. Jpn.* **66**, 1066 (1997).
32. P. J. Karaulis, *J. Appl. Crystallogr.* **24**, 946 (1991).
33. D. J. Bacon, W. F. Anderson, *J. Mol. Graph.* **6**, 219 (1988).
34. Supported by the NSF Focused Research Group on Fullerene Nanotube Chemistry (DMR-0073046), the NSF Center for Biological and Environmental Nanotechnology (EEC-0118007), and the Robert A. Welch Foundation (C-0689). Support from NASA (NCC 9-77) for development of the HiPco method is also gratefully acknowledged. R.B.W. and S.M.B. are grateful to the NSF (grant CHE-9900417) and the Robert A. Welch Foundation (grant C-0807) for research support. We thank R. Saito for communicating unpublished computational results.

8 April 2002; accepted 4 June 2002

Increase in the Asian Southwest Monsoon During the Past Four Centuries

David M. Anderson,^{1*} Jonathan T. Overpeck,² Anil K. Gupta³

Climate reconstructions reveal unprecedented warming in the past century; however, little is known about trends in aspects such as the monsoon. We reconstructed the monsoon winds for the past 1000 years using fossil *Globigerina bulloides* abundance in box cores from the Arabian Sea and found that monsoon wind strength increased during the past four centuries as the Northern Hemisphere warmed. We infer that the observed link between Eurasian snow cover and the southwest monsoon persists on a centennial scale. Alternatively, the forcing implicated in the warming trend (volcanic aerosols, solar output, and greenhouse gases) may directly affect the monsoon. Either interpretation is consistent with the hypothesis that the southwest monsoon strength will increase during the coming century as greenhouse gas concentrations continue to rise and northern latitudes continue to warm.

Major departures from normal seasonal rainfall seriously affect the agricultural output and economy of southwest Asia, which receives most of its annual rainfall during the summer monsoon season. Although decadal variations can be resolved in the instrumental record, little is known about centuries-long trends. Changes

in the monsoon over thousands to millions of years can be reconstructed using sediments from the northwestern Arabian Sea, where upwelling driven by the monsoon winds deposits a unique fossil record. Changes in the monsoon over millions of years have been attributed to uplift of the Tibetan Plateau, which altered the